

Steady-state response and free vibration of an embedded imperfect smart functionally graded hollow cylinder filled with compressible fluid

Z.G. Bian[†]

*Department of Civil Engineering, Ningbo Institute of Technology, Zhejiang University,
Ningbo 315100, P.R. China*

W.Q. Chen

Institute of Applied Mechanics, Zhejiang University, Hangzhou 310027, P.R. China

J. Zhao

Quzhou Highway Management Department, Quzhou 324000, P.R. China

(Received September 16, 2008, Accepted November 16, 2009)

Abstract. A smart hollow cylinder consisting of a host functionally graded elastic core layer and two surface homogeneous piezoelectric layers is presented in this paper. The bonding between the layers can be perfect or imperfect, depending on the parameters taken in the general linear spring-layer interface model. The effect of such weak interfaces on free vibration and steady-state response is then investigated. Piezoelectric layers at inner and outer surfaces are polarized axially or radially and act as a sensor and an actuator respectively. For a simply supported condition, the state equations with non-constant coefficients are obtained directly from the formulations of elasticity/piezoelectricity. An approximate laminated model is then introduced for the sake of solving the state equations conveniently. It is further assumed that the hollow cylinder is embedded in an elastic medium and is simultaneously filled with compressible fluid. The interaction between the structure and its surrounding media is taken into account. Numerical examples are finally given with discussions on the effect of some related parameters.

Keywords: free vibration; steady-state response; smart cylinder; interaction; imperfect interfaces; spring-layer model; state space approach.

1. Introduction

As a novel type of materials, functionally graded (FG) material occupies a continuous variation of material property, which is resulted from the continuously varying volume fraction of its components in certain directions. Since no elastic mismatch exists within the FG material, there is

[†] Ph.D., Corresponding author, E-mail: bzg@nit.net.cn

no or little stress concentration in FG structures (Mahmoud 2003). Nowadays, FG materials have been widely applied in medical industry (Pompe *et al.* 2003), aerospace industry (Gorokhovskiy *et al.* 2006, 2007) and nuclear industry (Ling *et al.* 2002), etc.

Piezoelectric material is another type of functional materials, in which coupling exists between the mechanical field and the electric field. Since the electric quantities can be measured and/or controlled conveniently, piezoelectric material has become the most widely applied smart material (Tiersten 1969, Tzou and Anderson 1992, Tzou 1993, Galassi *et al.* 2000). Most recently, Wilson *et al.* (2007) made a detailed discussion on the development of piezoelectric materials applied in micro-scale sensors and actuators.

Generally, the piezoelectric sensors and actuators are bonded to a host structure (Crawley and Luis 1987, Simões Moita *et al.* 2004). Because of the wide application of FG structures, their intelligentized character also becomes a concern. A lot of papers have been therefore published, studying the various characteristics of FG structures integrated with piezoelectric sensors and/or actuators. For example, Reddy and Cheng (2001) studied the bending of an FG rectangular plate attached with a piezoelectric actuator. Ray and Sachde (2006) developed a finite element model to analyze the static responses of an FG plate integrated with a piezoelectric layer. Huang and Shen (2006) investigated the nonlinear vibration and dynamic response of an FG plate bonded with piezoelectric layers in thermal environments. Kapuria *et al.* (2006) presented an assessment of coupled one-dimensional (1D) models for FG beams with bonded top and bottom piezoelectric surface layers.

In the literatures mentioned above, the piezoelectric layers were assumed to be perfectly bonded onto the host structures. In practice, the bonding between the FG structure and the piezoelectric layers may be imperfect during the fabrication process and the service life time (Aboudi 1987, Benveniste 1985), which can cause micro-defects (cracks, voids, inhomogeneities) and even delamination at the interfaces. Sun *et al.* (2001) discussed the effect of delamination on the vibration control of beams with piezoelectric sensors and actuators. Tan and Tong (2004, 2006) used an integrated piezoelectric sensor/actuator layer to identify the debonding in a composite beam. Della and Shu (2007) studied the influence of delaminated layers on the free vibration of a delaminated beam. For further publications, the reader is referred to the references cited in Lipton (2001), He and Lim (2003), and Rokhlin *et al.* (2004).

In history, there were two analytical models to describe the imperfect interface. One type employed Coulomb friction to deal with the load transfer at interfaces (Dollar and Steif 1988), the other type modeled the interfaces as elastic springs (Zhong and Folias 1992). Among the latter, the thickness of the interfaces was usually absent, and the linear spring-layer model was explored widely in literatures, e.g., Aboudi (1987), Achenbach and Zhu (1989), Pagano and Tandon (1990), Hashin (1990, 1991a, b), Qu (1993a, b) and Librescu and Schmidt (2001), etc.

In the present paper, the linear spring-layer model is also adopted to study the effect of imperfect interfaces on the steady-state response and free vibration characteristics of a smart hollow cylinder. Chen *et al.* (Chen *et al.* 2003, 2004b, c, 2006, Chen and Lee 2004, Bian *et al.* 2006a, b) have utilized this model in the three-dimensional exact investigations of laminated plates and shells. It is noted that the linear spring-layer model is not only convenient and effective for characterizing most important features of imperfect interfaces (Cheng *et al.* 1996), but also sufficiently precise at the initial stage of the interfacial debonding.

As a common structural type, solid and hollow cylinders are frequently encountered in areas of water supply, petroleum, ship, submarine, aerospace industry, etc. The response of cylinders can be

predicted by analytical methods based on various simplified theories (Botta and Cerri 2007, Haddadpour *et al.* 2007) or numerical methods (Ray and Reddy 2005, Shakeri *et al.* 2006). In certain applications, the cylindrical structures may be filled with and/or embedded in other media, and the interactions between the structure and its ambient media must be involved for the accurate prediction of its static and dynamic behavior (Junger and Feit 1993, Moore 2000). For the smart FG hollow cylinder considered in this paper, the FG material is inhomogeneous along the radial direction, the mechanical and electric fields in piezoelectric material are coupled, and there are interactions between the cylinder and the surrounding media, hence the analysis seems to be very complex. However, we will present a three-dimensional solution, which is directly based on the equations of elasticity or piezoelectricity. Such a solution is very important, because all elastic, dielectric and piezoelectric parameters are taken into account and it can be used to verify various simplified theories and numerical methods.

2. State space method

The smart hybrid hollow cylinder is displayed in Fig. 1, where a host FG elastic layer is integrated with two inner and outer piezoelectric layers. The FG material is inhomogeneous along the radial direction, while the piezoelectric material is homogeneous. Thicknesses of the three layers are H_1 , H_2 and H_3 , respectively, and H ($= H_1 + H_2 + H_3$) is the total thickness of the smart hollow cylinder. Besides, L and R represent the length and inner radius, respectively.

2.1 Formulations for piezoelectric sensor and actuator

In cylindrical coordinates (r, θ, z) , the basic equations of orthotropic piezoelectric materials are as follows (Ding and Chen 2001).

Generalized geometric equations

$$\begin{aligned} \varepsilon_{rr} &= \frac{\partial u_r}{\partial r}, \quad \varepsilon_{\theta\theta} = \frac{\partial u_\theta}{r\partial\theta} + \frac{u_r}{r}, \quad \varepsilon_{zz} = \frac{\partial u_z}{\partial z}, \quad E_r = -\frac{\partial\Phi}{\partial r}, \quad E_\theta = -\frac{\partial\Phi}{r\partial\theta}, \quad E_z = -\frac{\partial\Phi}{\partial z} \\ \varepsilon_{r\theta} &= \frac{1}{2}\left(\frac{\partial u_r}{r\partial\theta} + \frac{\partial u_\theta}{\partial r} - \frac{u_\theta}{r}\right), \quad \varepsilon_{\theta z} = \frac{1}{2}\left(\frac{\partial u_\theta}{\partial z} + \frac{\partial u_z}{r\partial\theta}\right), \quad \varepsilon_{zr} = \frac{1}{2}\left(\frac{\partial u_z}{\partial r} + \frac{\partial u_r}{\partial z}\right) \end{aligned} \quad (1)$$

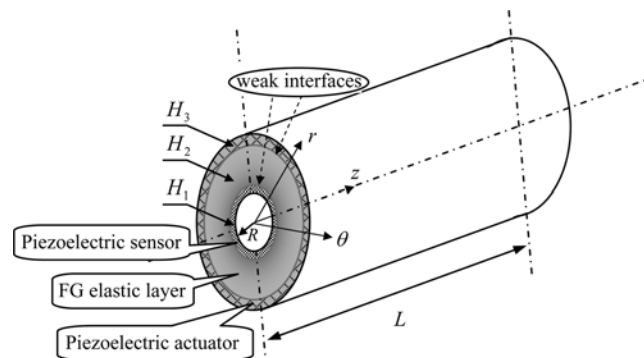


Fig. 1 Model of a smart cylinder

Equations of motion and equilibrium equation of electrostatics

$$\begin{aligned}
 \frac{\partial \sigma_{zz}}{\partial z} + \frac{1}{r} \frac{\partial \sigma_{\theta z}}{\partial \theta} + \frac{\partial \sigma_{zr}}{\partial r} + \frac{\sigma_{rz}}{r} + f_z &= \rho \frac{\partial^2 u_z}{\partial t^2} \\
 \frac{\partial \sigma_{\theta z}}{\partial z} + \frac{1}{r} \frac{\partial \sigma_{\theta\theta}}{\partial \theta} + \frac{\partial \sigma_{r\theta}}{\partial r} + \frac{2\sigma_{r\theta}}{r} + f_\theta &= \rho \frac{\partial^2 u_\theta}{\partial t^2} \\
 \frac{\partial \sigma_{zr}}{\partial z} + \frac{1}{r} \frac{\partial \sigma_{r\theta}}{\partial \theta} + \frac{\partial \sigma_{rr}}{\partial r} + \frac{\sigma_{rr} - \sigma_{\theta\theta}}{r} + f_r &= \rho \frac{\partial^2 u_r}{\partial t^2} \\
 \frac{\partial D_r}{\partial r} + \frac{1}{r} \frac{\partial D_\theta}{\partial \theta} + \frac{\partial D_z}{\partial z} + \frac{D_r}{r} &= \rho_f
 \end{aligned} \tag{2}$$

where u_k, f_k, E_k and D_k ($k = r, \theta, z$) are components of mechanical displacement, body force, electric intensity and electric displacement, respectively; σ_{kl} and ε_{kl} ($k, l = r, \theta, z$) represent components of stress and strain, respectively; ρ is the mass density of the piezoelectric material; Φ and ρ_f are the electric potential and the free charge density, respectively.

The generalized constitutive relations are different for different polarizations. In this paper, both the axially polarized (AP) piezoelectrics and the radially polarized (RP) piezoelectrics are considered.

Generalized constitutive relations for AP

$$\begin{aligned}
 \sigma_{rr} &= c_{11}\varepsilon_{rr} + c_{12}\varepsilon_{\theta\theta} + c_{13}\varepsilon_{zz} - e_{31}E_z, \quad \sigma_{\theta\theta} = c_{12}\varepsilon_{rr} + c_{22}\varepsilon_{\theta\theta} + c_{23}\varepsilon_{zz} - e_{32}E_z \\
 \sigma_{zz} &= c_{13}\varepsilon_{rr} + c_{23}\varepsilon_{\theta\theta} + c_{33}\varepsilon_{zz} - e_{33}E_z \\
 \sigma_{\theta z} &= 2c_{44}\varepsilon_{\theta z} - e_{24}E_\theta, \quad \sigma_{zr} = 2c_{55}\varepsilon_{zr} - e_{15}E_r, \quad \sigma_{r\theta} = 2c_{66}\varepsilon_{r\theta} \\
 D_r &= 2e_{15}\varepsilon_{zr} + \chi_{11}E_r, \quad D_\theta = 2e_{24}\varepsilon_{\theta z} + \chi_{22}E_\theta, \quad D_z = e_{31}\varepsilon_{rr} + e_{32}\varepsilon_{\theta\theta} + e_{33}\varepsilon_{zz} + \chi_{33}E_z
 \end{aligned} \tag{3a}$$

Generalized constitutive relations for RP

$$\begin{aligned}
 \sigma_{\theta\theta} &= c_{11}\varepsilon_{\theta\theta} + c_{12}\varepsilon_{zz} + c_{13}\varepsilon_{rr} - e_{31}E_r, \quad \sigma_{zz} = c_{12}\varepsilon_{\theta\theta} + c_{22}\varepsilon_{zz} + c_{23}\varepsilon_{rr} - e_{32}E_r \\
 \sigma_{rr} &= c_{13}\varepsilon_{\theta\theta} + c_{23}\varepsilon_{zz} + c_{33}\varepsilon_{rr} - e_{33}E_r \\
 \sigma_{zr} &= 2c_{44}\varepsilon_{zr} - e_{24}E_z, \quad \sigma_{r\theta} = 2c_{55}\varepsilon_{r\theta} - e_{15}E_\theta, \quad \sigma_{\theta z} = 2c_{66}\varepsilon_{\theta z} \\
 D_\theta &= 2e_{15}\varepsilon_{r\theta} + \chi_{11}E_\theta, \quad D_z = 2e_{24}\varepsilon_{zr} + \chi_{22}E_z, \quad D_r = e_{31}\varepsilon_{\theta\theta} + e_{32}\varepsilon_{zz} + e_{33}\varepsilon_{rr} + \chi_{33}E_r
 \end{aligned} \tag{3b}$$

where c_{ij} , χ_{ij} and e_{ij} ($i, j = 1, 2, \dots, 6$) are the elastic, dielectric and piezoelectric constants, respectively.

From Eqs. (1) to (3), the state equations can be directly derived by following a routine way (Ding and Chen 2001). In absence of body force and free charge density, they are

$$\partial \mathbf{Y} / \partial r = \mathbf{M} \mathbf{Y} \tag{4}$$

where $\mathbf{Y} = [u_z \ u_\theta \ \sigma_{rr} \ D_r \ \sigma_{zr} \ \sigma_{r\theta} \ u_r \ \Phi]^T$ is as the so-called state vector, and \mathbf{M} is an operational matrix, whose expression is given in Appendix and is different for AP and RP.

In addition, the derived vector, $\mathbf{X} = [\sigma_{zz} \ \sigma_{\theta\theta} \ \sigma_{\theta z} \ D_z \ D_\theta]^T$, can be written as

$$\mathbf{X} = \mathbf{N}\mathbf{Y} \tag{5}$$

where \mathbf{N} is also an operational matrix presented in Appendix.

Suppose that the piezoelectric cylinder is simply supported at $z = 0$ and L . The mechanical boundary conditions at the two ends are (Ding and Chen 2001)

$$u_r = 0, \quad u_\theta = 0, \quad \sigma_{zz} = 0 \tag{6}$$

In the light of Eqs. (1), (3) and (6), one can expand the state vector \mathbf{Y} as

$$\mathbf{Y} = \sum_{m=0}^{\infty} \sum_{n=0}^{\infty} \left\{ \begin{array}{l} R\bar{u}_z(\eta) \cos(m\pi\zeta) \cos(n\theta) \\ R\bar{u}_\theta(\eta) \sin(m\pi\zeta) \sin(n\theta) \\ c_{44}^s \bar{\sigma}_{rr}(\eta) \sin(m\pi\zeta) \cos(n\theta) \\ \sqrt{c_{44}^s \chi_{33}^s} \bar{D}_r(\eta) \sin(m\pi\zeta + \varphi_0) \cos(n\theta) \\ c_{44}^s \bar{\sigma}_{zr}(\eta) \cos(m\pi\zeta) \cos(n\theta) \\ c_{44}^s \bar{\sigma}_{r\theta}(\eta) \sin(m\pi\zeta) \sin(n\theta) \\ R\bar{u}_r(\eta) \sin(m\pi\zeta) \cos(n\theta) \\ R\sqrt{c_{44}^s / \chi_{33}^s} \bar{\Phi}(\eta) \sin(m\pi\zeta + \varphi_0) \cos(n\theta) \end{array} \right\} \exp(i\omega t) \tag{7}$$

where $\eta = r/R$ and $\zeta = z/L$; m and n are the axial half-wave number and circumferential wave number, respectively; ω is the circular frequency; φ_0 equals to $\pi/2$ or 0 for AP and for RP, respectively; c_{44}^s and χ_{33}^s are the corresponding material constants of piezoelectric sensor. The overbar on each quantity corresponds to a dimensionless quantity.

At the simply supported ends, the electric boundary conditions are (Ding and Chen 2001)

$$D_z = 0, \quad \Phi \neq 0 \quad \text{for AP} \tag{8a}$$

$$D_z \neq 0, \quad \Phi = 0 \quad \text{for RP} \tag{8b}$$

The substitution of Eq. (7) into Eq. (4) leads to

$$\frac{d}{d\eta} \bar{\mathbf{Y}} = \mathbf{D} \bar{\mathbf{Y}} \tag{9}$$

where $\mathbf{Y} = [\bar{u}_z \ \bar{u}_\theta \ \bar{\sigma}_{rr} \ \bar{D}_r \ \bar{\sigma}_{zr} \ \bar{\sigma}_{r\theta} \ \bar{u}_r \ \bar{\Phi}]^T$ is a dimensionless state vector, and \mathbf{D} is an eighth-order coefficient matrix, which is given in Appendix.

2.2 Formulations for FG elastic layer

The state equation for an FG elastic layer can be derived in a similar way from the basic equations for elastic material as

$$\frac{d}{d\eta} \bar{\mathbf{Y}}^f = \mathbf{D}^f \bar{\mathbf{Y}}^f \tag{10}$$

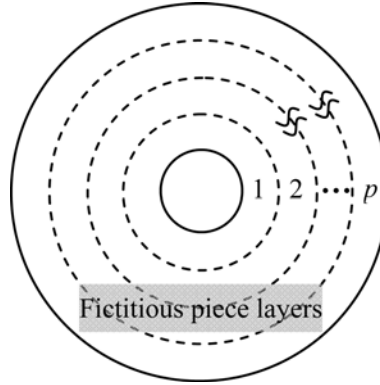


Fig. 2 An approximate laminated model for a cylinder

where $\bar{\mathbf{Y}}^f = [\bar{u}_z \ \bar{u}_\theta \ \bar{\sigma}_{rr} \ \bar{\sigma}_{zr} \ \bar{\sigma}_{r\theta} \ \bar{u}_r]^T$ is the dimensionless state vector for the FG elastic layer, and \mathbf{D}^f is a sixth-order coefficient matrix, which can be obtained by letting e_{ij} vanish along with deleting the fourth and eighth rows and columns of \mathbf{D} in Eq. (9).

2.3 Solution to state equations

The coefficient matrices, \mathbf{D}^f and \mathbf{D} , are still r -dependent, and hence it is difficult to solve Eqs. (9) and (10) directly. Herein an approximate laminated model (Chen *et al.* 2004a) is adopted. That is, the cylinder is equally divided into many fictitious thin layers, as shown in Fig. 2. The \mathbf{D}^f or \mathbf{D} approximates to take its value at the middle surface of each layer. Now Eqs. (9) and (10) can be solved readily. Suppose the inner and outer piezoelectric layers act as sensor and actuator respectively. The solution in a certain layer (e.g., the j th layer) is

For the piezoelectric sensor ($1 \leq \eta \leq \eta_1 = 1 + H_1/R$)

$$\bar{\mathbf{Y}}^s(\eta) = \exp[(\eta - \eta_j^0)\mathbf{D}_j^s]\bar{\mathbf{Y}}^s(\eta_j^0), \quad \eta_j^0 = 1 + \frac{j-1}{p_1} \frac{H_1}{R} \leq \eta \leq \eta_j^1 = 1 + \frac{j}{p_1} \frac{H_1}{R}$$

For the FG elastic layer ($\eta_1 \leq \eta \leq \eta_2 = \eta_1 + H_2/R$)

$$\bar{\mathbf{Y}}^f(\eta) = \exp[(\eta - \eta_j^0)\mathbf{D}_j^f]\bar{\mathbf{Y}}^f(\eta_j^0), \quad \eta_j^0 = \eta_1 + \frac{j-1}{p_2} \frac{H_2}{R} \leq \eta \leq \eta_j^1 = \eta_1 + \frac{j}{p_2} \frac{H_2}{R} \quad (11)$$

For the piezoelectric actuator ($\eta_2 \leq \eta \leq \eta_3 = \eta_2 + H_3/R$)

$$\bar{\mathbf{Y}}^a(\eta) = \exp[(\eta - \eta_j^0)\mathbf{D}_j^a]\bar{\mathbf{Y}}^a(\eta_j^0), \quad \eta_j^0 = \eta_2 + \frac{j-1}{p_3} \frac{H_3}{R} \leq \eta \leq \eta_j^1 = \eta_2 + \frac{j}{p_3} \frac{H_3}{R}$$

where (and hereafter) the superscripts 's' and 'a' on $\bar{\mathbf{Y}}$ and \mathbf{D} denote the quantities for piezoelectric sensor and actuator respectively; p_1 , p_2 and p_3 are the numbers of fictitious layers of the piezoelectric sensor, the FG elastic layer and the piezoelectric actuator, respectively.

From Eq. (11), the following transfer relations can be obtained since the state vectors are continuous at the interfaces between any two adjacent fictitious layers

$$\begin{aligned}
\bar{\mathbf{Y}}^s(\eta_1) &= \mathbf{T}^s \bar{\mathbf{Y}}^s(1), & \mathbf{T}^s &= \prod_{j=p_1}^1 \exp\left(\frac{\mathbf{D}_j^s}{p_1} \cdot \frac{H_1}{R}\right) \\
\bar{\mathbf{Y}}^f(\eta_2) &= \mathbf{T}^f \bar{\mathbf{Y}}^f(\eta_1), & \mathbf{T}^f &= \prod_{j=p_2}^1 \exp\left(\frac{\mathbf{D}_j^f}{p_2} \cdot \frac{H_2}{R}\right) \\
\bar{\mathbf{Y}}^a(\eta_3) &= \mathbf{T}^a \bar{\mathbf{Y}}^a(\eta_2), & \mathbf{T}^a &= \prod_{j=p_3}^1 \exp\left(\frac{\mathbf{D}_j^a}{p_3} \cdot \frac{H_3}{R}\right)
\end{aligned} \tag{12}$$

3. Linear spring model for imperfect interfaces

To take account of the imperfect bonding at interfaces between the piezoelectric layers and the FG layer, a general linear spring model (Chen *et al.* 2003) is employed, which leads to the following relationships,

At the interface between piezoelectric sensor and the FG layer (inner interface, $\eta = \eta_1$)

$$\begin{aligned}
\sigma_{r\theta}^s(\eta_1) &= \sigma_{r\theta}^f(\eta_1) = [u_{\theta}^f(\eta_1) - u_{\theta}^s(\eta_1)]/R_{\theta}^s \\
\sigma_{zr}^s(\eta_1) &= \sigma_{zr}^f(\eta_1) = [u_z^f(\eta_1) - u_z^s(\eta_1)]/R_z^s \\
\sigma_{rr}^s(\eta_1) &= \sigma_{rr}^f(\eta_1) = [u_r^f(\eta_1) - u_r^s(\eta_1)]/R_r^s
\end{aligned}$$

At the interface between piezoelectric actuator and the FG layer (outer interface, $\eta = \eta_2$)

$$\begin{aligned}
\sigma_{r\theta}^a(\eta_2) &= \sigma_{r\theta}^f(\eta_2) = [u_{\theta}^a(\eta_2) - u_{\theta}^f(\eta_2)]/R_{\theta}^a \\
\sigma_{zr}^a(\eta_2) &= \sigma_{zr}^f(\eta_2) = [u_z^a(\eta_2) - u_z^f(\eta_2)]/R_z^a \\
\sigma_{rr}^a(\eta_2) &= \sigma_{rr}^f(\eta_2) = [u_r^a(\eta_2) - u_r^f(\eta_2)]/R_r^a
\end{aligned} \tag{13}$$

where the superscript 'f' denotes quantities of the FG elastic layer; and R_k^i ($k = r, \theta, z; i = s, a$) are the compliance coefficients of bonding adhesives at the interfaces. Obviously, the present model also represents several particular cases of weak interfaces as different values of R_k^i are assigned. For example, the complete slip-type imperfection can be modeled by setting R_r^i to zero as well as assigning R_{θ}^i and R_z^i to infinite. When all R_k^i are assigned to be zero or infinity, the model represents the completely perfect or completely delaminated interfaces respectively. The small values of R_k^i imply a slightly imperfect interface, which may be caused by micro-cracks, voids, fatigue damage and so on.

Combing Eq. (7) with Eq. (13), one can obtain

$$\bar{\mathbf{Y}}^f(\eta_1) = \mathbf{P}^s \bar{\mathbf{Y}}_m^s(\eta_1), \quad \bar{\mathbf{Y}}_m^a(\eta_2) = \mathbf{P}^a \bar{\mathbf{Y}}^f(\eta_2) \tag{14}$$

where $\bar{\mathbf{Y}}_m^s$ and $\bar{\mathbf{Y}}_m^a$ are the mechanical part of $\bar{\mathbf{Y}}^s$ and $\bar{\mathbf{Y}}^a$ respectively; $\bar{\mathbf{Y}}_m = [\bar{u}_z \quad \bar{u}_{\theta} \quad \bar{\sigma}_{rr} \quad \bar{\sigma}_{zr} \quad \bar{\sigma}_{r\theta} \quad \bar{u}_r]^T$; \mathbf{P}^s and \mathbf{P}^a are the compliance matrixes defined by

$$\mathbf{P}^s = \begin{bmatrix} 1 & 0 & 0 & \frac{R_z^s c_{44}^s}{R} & 0 & 0 \\ 0 & 1 & 0 & 0 & \frac{R_\theta^s c_{44}^s}{R} & 0 \\ 0 & 0 & 1 & 0 & 0 & 0 \\ 0 & 0 & 0 & 1 & 0 & 0 \\ 0 & 0 & 0 & 0 & 1 & 0 \\ 0 & 0 & \frac{R_r^s c_{44}^s}{R} & 0 & 0 & 1 \end{bmatrix}, \quad \mathbf{P}^a = \begin{bmatrix} 1 & 0 & 0 & \frac{R_z^a c_{44}^a}{R} & 0 & 0 \\ 0 & 1 & 0 & 0 & \frac{R_\theta^a c_{44}^a}{R} & 0 \\ 0 & 0 & 1 & 0 & 0 & 0 \\ 0 & 0 & 0 & 1 & 0 & 0 \\ 0 & 0 & 0 & 0 & 1 & 0 \\ 0 & 0 & \frac{R_r^a c_{44}^a}{R} & 0 & 0 & 1 \end{bmatrix} \quad (15)$$

As mentioned above, R_k^i vanishes for the perfect interface, and accordingly the compliance matrices become identity matrices.

4. Boundary conditions of piezoelectric layers and the global governing equation

4.1 Electric boundary conditions of piezoelectric sensor and actuator

For the piezoelectric actuator, a voltage difference is imposed between its inner and outer surfaces. Thus, the electric boundary conditions are (Bian *et al.* 2006a, b)

$$\Phi = \Phi^{(1)}(\zeta, \theta)\exp(i\omega t) \text{ at } \eta = \eta_3, \text{ and } \Phi = \Phi^{(2)}(\zeta, \theta)\exp(i\omega t) \text{ at } \eta = \eta_2 \quad (16)$$

where ω is the circular frequency of the imposed electric potentials, and $\Phi^{(k)}(\zeta, \theta)$ ($k = 1$ and 2 for $\eta = \eta_3$ and $\eta = \eta_2$, respectively) are the amplitudes, which can be expanded as

$$\Phi^{(k)}(\zeta, \theta) = \sum_{m=0}^{\infty} \sum_{n=0}^{\infty} R \sqrt{c_{44}^s / \chi_{33}^s} f_{mn}^{(k)} \sin(m\pi\zeta + \varphi_0) \cos(n\theta) \quad (17)$$

where

$$f_{mn}^{(k)} = \frac{4}{R \sqrt{c_{44}^s / \chi_{33}^s}} \int_0^1 \int_0^1 \Phi^{(k)}(\zeta, \theta) \sin(m\pi\zeta + \varphi_0) \cos(n\theta) d\zeta d\theta \quad (18)$$

are the Fourier coefficients.

Incorporating Eq. (16) with Eq. (12) yields

$$\begin{aligned} \bar{D}_r(\eta_2) &= \frac{f_{mn}^{(1)} - T_{88}^a f_{mn}^{(2)}}{T_{84}^a} - \frac{1}{T_{84}^a} [T_{81}^a \ T_{82}^a \ T_{83}^a \ T_{85}^a \ T_{86}^a \ T_{87}^a] \bar{\mathbf{Y}}_m^a(\eta_2) \\ \bar{\mathbf{Y}}_m^a(\eta_3) &= \left\{ [\mathbf{C}_1^a \ \mathbf{C}_2^a \ \mathbf{C}_3^a \ \mathbf{C}_5^a \ \mathbf{C}_6^a \ \mathbf{C}_7^a] - \frac{1}{T_{84}^a} \mathbf{C}_4^a \mathbf{R}_8^a \right\} \bar{\mathbf{Y}}_m^a(\eta_2) + \frac{f_{mn}^{(1)} - T_{88}^a f_{mn}^{(2)}}{T_{84}^a} \mathbf{C}_4^a + f_{mn}^{(2)} \mathbf{C}_8^a \end{aligned} \quad (19)$$

where T_{ij}^a are elements of matrix \mathbf{T}^a , $\mathbf{C}_i^a = [T_{1i}^a \ T_{2i}^a \ T_{3i}^a \ T_{5i}^a \ T_{6i}^a \ T_{7i}^a]^T$ and $\mathbf{R}_i^a = [T_{i1}^a \ T_{i2}^a \ T_{i3}^a \ T_{i5}^a \ T_{i6}^a \ T_{i7}^a]^T$.

The electric boundary conditions of the piezoelectric sensor are open-circuit and closed-circuit (grounded) at its inner and outer surfaces respectively, i.e.

$$\Phi = 0 \text{ at } \eta = \eta_1, \quad D_r = 0 \text{ at } \eta = 1 \quad (20)$$

In a similar manner, the following formulas can be derived

$$\begin{aligned} \bar{\Phi}(1) &= -\frac{1}{T_{88}^s} [T_{81}^s \ T_{82}^s \ T_{83}^s \ T_{85}^s \ T_{86}^s \ T_{87}^s] \bar{\mathbf{Y}}_m^s(1) \\ \bar{\mathbf{Y}}_m^s(\eta_1) &= \left\{ [\mathbf{C}_1^s \ \mathbf{C}_2^s \ \mathbf{C}_3^s \ \mathbf{C}_5^s \ \mathbf{C}_6^s \ \mathbf{C}_7^s] - \frac{1}{T_{88}^s} \mathbf{C}_8^s \mathbf{R}_8^s \right\} \bar{\mathbf{Y}}_m^s(1) \end{aligned} \quad (21)$$

where T_{ij}^s are elements of matrix \mathbf{T}^s , $\mathbf{C}_i^s = [T_{1i}^s \ T_{2i}^s \ T_{3i}^s \ T_{5i}^s \ T_{6i}^s \ T_{7i}^s]^T$ and $\mathbf{R}_i^s = [T_{i1}^s \ T_{i2}^s \ T_{i3}^s \ T_{i5}^s \ T_{i6}^s \ T_{i7}^s]$.

Making use of Eqs. (12), (14), (19) and (21), we obtain the global transfer relation for the elastic field

$$\bar{\mathbf{Y}}_m^a(\eta_3) = \mathbf{S} \bar{\mathbf{Y}}_m^s(1) + \mathbf{B} \quad (22)$$

where

$$\begin{aligned} \mathbf{S} &= \left\{ [\mathbf{C}_1^a \ \mathbf{C}_2^a \ \mathbf{C}_3^a \ \mathbf{C}_5^a \ \mathbf{C}_6^a \ \mathbf{C}_7^a] - \frac{1}{T_{84}^a} \mathbf{C}_4^a \mathbf{R}_8^a \right\} \times \mathbf{P}^a \mathbf{T}^a \mathbf{P}^s \times \left\{ [\mathbf{C}_1^s \ \mathbf{C}_2^s \ \mathbf{C}_3^s \ \mathbf{C}_5^s \ \mathbf{C}_6^s \ \mathbf{C}_7^s] - \frac{1}{T_{88}^s} \mathbf{C}_8^s \mathbf{R}_8^s \right\} \\ \mathbf{B} &= \frac{f_{mn}^{(1)} - T_{88}^a f_{mn}^{(2)}}{T_{84}^a} \mathbf{C}_4^a + f_{mn}^{(2)} \mathbf{C}_8^a \end{aligned} \quad (23)$$

4.2 Mechanical boundary conditions on the inner and outer surfaces

Suppose that the hybrid hollow cylinder is fully filled with compressible, non-viscous fluid. The mechanical boundary conditions at the fluid-solid interface are (Chen *et al.* 2004)

$$\sigma_{r\theta} = 0, \quad \sigma_{zr} = 0, \quad \sigma_{rr} = -\omega^2 R \cdot \rho^l \cdot u_r \cdot Q(\eta) \quad (24)$$

where ρ^l is the mass density of the fluid ($\rho^l = 0$ corresponds to the case of empty hollow cylinder), and $Q(\eta)$ is defined as

$$Q(\eta) = \begin{cases} \frac{J_n(v\eta)}{J_{n-1}(v\eta) - J_{n+1}(v\eta)} \cdot \frac{2}{v}, & v^2 > 0 \\ \frac{\eta}{n}, & v^0 = 0 \\ \frac{I_n(\tilde{v}\eta)}{I_{n-1}(\tilde{v}\eta) + I_{n+1}(\tilde{v}\eta)} \cdot \frac{2}{\tilde{v}}, & v^2 = -\tilde{v}^2 < 0 \end{cases} \quad (25)$$

where J_n and I_n are the Bessel function and the modified Bessel function of the first kind, respectively, and $v^2 = (c^s/c^l)^2 \Omega^2 - \lambda^2$, in which c^l is the sound velocity in the fluid and $c^s = \sqrt{c_{44}^s/\rho^s}$ is the velocity of elastic wave in the sensor.

Substituting Eq. (7) into Eq. (24), we can express the boundary conditions on the inner cylindrical surface as

$$\bar{\sigma}_{r\theta} = 0, \quad \bar{\sigma}_{zr} = 0 \quad \text{and} \quad \bar{\sigma}_{rr} = -\wp \bar{u}_r \quad \text{at} \quad \eta = 1 \quad (26)$$

where $\wp = \Omega^2 Q(1) \rho^l / \rho^s$

We further suppose that the hollow cylinder is embedded in an elastic medium, which is treated as the Pasternak model. The boundary conditions on the outer surface therefore are

$$\sigma_{r\theta} = 0, \quad \sigma_{zr} = 0 \quad \text{and} \quad \sigma_{rr} = -Ku_r + G\nabla u_r \quad \text{at} \quad \eta = \eta_3 \quad (27)$$

where $\nabla = \partial^2 / \partial z^2 + (1/r^2) \partial^2 / \partial \theta^2$, K and G are the elastic modulus and the shear modulus of the foundation, respectively. It is mentioned here that the elastic foundation will become the Winkler type if setting $G = 0$ in Eq. (27).

Substitution of Eq. (7) into Eq. (27) gives

$$\bar{\sigma}_{r\theta} = 0, \quad \bar{\sigma}_{zr} = 0 \quad \text{and} \quad \bar{\sigma}_{rr} = -\wp \bar{u}_r \quad \text{at} \quad \eta = \eta_3 \quad (28)$$

where $\wp = KR/c_{44}^s + [\lambda^2 + (n/\eta_3)^2]G/(Rc_{44}^s)$.

4.3 Governing equation

From Eqs. (22), (26) and (28), the following system of equations can be derived

$$\begin{bmatrix} S_{41} & S_{42} & S_{46} - \wp S_{43} \\ S_{51} & S_{52} & S_{56} - \wp S_{53} \\ S_{31} + \wp S_{61} & S_{32} + \wp S_{62} & \wp(S_{66} - \wp S_{63}) + S_{36} - \wp S_{33} \end{bmatrix} \begin{Bmatrix} \bar{u}_z(1) \\ \bar{u}_\theta(1) \\ \bar{u}_r(1) \end{Bmatrix} = - \begin{Bmatrix} B_4 \\ B_5 \\ B_3 + \wp B_6 \end{Bmatrix} \quad (29)$$

where S_{ij} and B_i are elements of matrix \mathbf{S} and vector \mathbf{B} , respectively. Then the governing equation for a steady-state response of the hybrid hollow cylinder is deduced

$$\begin{Bmatrix} \bar{u}_z(1) \\ \bar{u}_\theta(1) \\ \bar{u}_r(1) \end{Bmatrix} = - \begin{bmatrix} S_{41} & S_{42} & S_{46} - \wp S_{43} \\ S_{51} & S_{52} & S_{56} - \wp S_{53} \\ S_{31} + \wp S_{61} & S_{32} + \wp S_{62} & \wp(S_{66} - \wp S_{63}) + S_{36} - \wp S_{33} \end{bmatrix}^{-1} \begin{Bmatrix} B_4 \\ B_5 \\ B_3 + \wp B_6 \end{Bmatrix} \quad (30)$$

From Eq. (30), the displacement components and subsequently the mechanical state vector, $\bar{\mathbf{Y}}_m^s(1) = [\bar{u}_z(1), \bar{u}_\theta(1) - \wp \bar{u}_r(1), 0, 0, \bar{u}_r(1)]^T$ can be determined. Now the three basic state vectors, $\bar{\mathbf{Y}}^s(1)$, $\bar{\mathbf{Y}}^a(\eta_1)$ and $\bar{\mathbf{Y}}^a(\eta_2)$ can be solved by the virtue of Eqs. (12), (14), (19) and (21). Finally, the state vector at any position can be determined from Eq. (11).

The frequency equation can be also derived from Eq. (29). For free vibration, the piezoelectric actuator is grounded, i.e., $f_{mn}^{(k)} = 0$. Thus we have $\mathbf{B} = \mathbf{0}$ and Eq. (29) becomes homogeneous. For non-trivial solution to exist, the determinant of the coefficient matrix in Eq. (29) must vanish, i.e.

$$\begin{vmatrix} S_{41} & S_{42} & S_{46} - \wp S_{43} \\ S_{51} & S_{52} & S_{56} - \wp S_{53} \\ S_{31} + \wp S_{61} & S_{32} + \wp S_{62} & \wp(S_{66} - \wp S_{63}) + S_{36} - \wp S_{33} \end{vmatrix} = 0 \quad (31)$$

Table 1 Material constants of two homogenous materials of the FG elastic layer

Property	Young's modulus E (GPa)	Poisson's ratio ν	Mass density ρ (kg/m ³)
P_i (Ti-6Al-4V)	110	0.30	4500
P_o (SiC)	440	0.25	2700

Table 2 Material constants of piezoelectric sensor and actuator (Units: c_{ij} -10¹⁰ N/m², χ_{ij} -10⁻¹¹ F/m, e_{ij} -C/m², ρ -kg/m³)

Property	c_{11}	c_{12}	c_{13}	c_{22}	c_{23}	c_{33}	c_{44}	c_{55}	c_{66}
Piezoelectric sensor (PVDF)	0.361	0.161	0.142	0.313	0.131	0.163	0.055	0.059	0.069
Piezoelectric actuator (PZT-4)	13.9	7.78	7.43	13.9	7.43	11.5	2.56	2.56	3.06
Property	e_{15}	e_{24}	e_{31}	e_{32}	e_{33}	χ_{11}	χ_{22}	χ_{33}	ρ
Piezoelectric sensor (PVDF)	-15.93 $\times 10^{-3}$	-12.65 $\times 10^{-3}$	32.075 $\times 10^{-3}$	-4.07 $\times 10^{-3}$	-21.19 $\times 10^{-3}$	5.4	6.64	5.93	1800
Piezoelectric actuator (PZT-4)	12.7	12.7	-5.2	-5.2	15.1	646.4	646.4	562.2	7500

5. Numerical examples

The steady-state response and the free vibration of the hybrid hollow cylinder are studied numerically in this section. Suppose that the thickness ratio is $H_1:H_2:H_3 = 1:2:1$ and the total thickness-to-inner radius ratio is $H/R = 1$. For the FG layer, a widely adopted model on distribution of material properties (Chen *et al.* 2004a) is also adopted here

$$P(\eta) = P_o \left(\frac{\eta - \eta_1}{\eta_2 - \eta_1} \right)^\kappa + P_i \left[1 - \left(\frac{\eta - \eta_1}{\eta_2 - \eta_1} \right)^\kappa \right] \quad (\eta_1 \leq \eta \leq \eta_2) \quad (32)$$

where κ is a gradient index, P represents an arbitrary material constant of the FG material, while P_i and P_o refer to the corresponding ones of two homogeneous materials, which are Ti-6Al-4V and SiC respectively in this paper. The material constants of these two homogeneous materials are listed in Table 1. Note that the two materials are isotropic, so that the elastic constant c_{ij} should be calculated according to the well-known formulae from Young's modulus and Poisson's ratio (Ding and Chen 2001). Table 2 gives the material constants of the piezoelectric sensor and actuator, which are PVDF and PZT-4 respectively. It is also assumed that the parameters of the outer elastic foundation are $KR/c_{44}^s = 0.1$ and $G/(Rc_{44}^s) = 0.01$. Except for special explanation, the filled fluid is water, whose sound velocity (c^f) is 1430 m/s (15°C) and the mass density (ρ) is 1000 kg/m³.

To avoid the phenomenon of material penetration at the two interfaces (Bian *et al.* 2006a, b), we assume $R_r^s = R_r^a = 0$ in the following numerical examples. Also we suppose $R_\theta^s = R_\theta^a$ and $R_z^s = R_z^a$ for brevity. Two dimensionless parameters are further introduced as $\bar{R}_\theta = R_\theta^s c_{44}^s / R$ and $\bar{R}_z = R_z^s c_{44}^s / R$.

Though the compliance coefficients can be determined by means of theoretical evaluations and experimental measurements (Cheng *et al.* 1996), the purpose here is just to test the effect of

imperfect interfaces on the response characteristics of a hybrid cylinder. So some small values of \bar{R}_θ and \bar{R}_z are chosen hereunder.

5.1 Discussion on particular modes of free vibration

When some special values of wave numbers are chosen, some particular models of free vibrations occur. In the following, we will make a brief discussion on these modes, since which are important in practical applications.

- (1) $m = 0, n = 0$. From Eqs. (5) and (7), we can find that all the mechanical quantities vanish except for u_z and σ_{zr} , which only depends on $r(\eta)$. This corresponds to the axisymmetric longitudinal-shear vibration mode.
- (2) $m = 0, n \neq 0$. The nonzero mechanical quantities are $u_z, \sigma_{\theta z}$ and σ_{zr} , which are independent of $z(\zeta)$. It is the non-axisymmetric longitudinal-shear vibration mode.
- (3) $m \neq 0, n = 0$. Only $u_\theta, \sigma_{r\theta}$ and $\sigma_{\theta z}$ vanish, and all other physical variables are independent of θ . It is the axisymmetric flexural vibration mode.
- (4) Interchanging $\cos(n\theta)$ and $\sin(n\theta)$ in Eq. (7), we can find that the solution still satisfies the simply supported conditions at the ends along the axial direction. If $m \neq 0$ and $n = 0$, then only $u_\theta, \sigma_{r\theta}$ and $\sigma_{\theta z}$ are nonzero, and all other quantities are independent of θ . It is the pure torsional vibration mode.

Among the above cases, only the axisymmetric flexural vibration (Case 3) involves interactions with the inner fluid and the outer elastic medium. When $m \neq 0$ and $n \neq 0$, the vibration is the most general flexural one, which is to be discussed in detail.

5.2 Free vibration

First of all, the convergence characteristic of the present method employing the laminated model is to be numerically verified. Table 3 gives the nondimensional natural frequencies Ω ($= \omega R \sqrt{\rho^s / c_{44}^s}$) with different numbers of fictitious layers, where $3p_1 = p_2 = 3p_3$, and $p = p_1 + p_2 + p_3$ is the total number. The other parameters are $m = n = 1$, $\kappa = 1$, $\bar{R}_\theta = \bar{R}_z = 0.5$, and both the piezoelectric sensor and actuator are RP. It is immediately seen that all the difference between the results of $p = 90$ and 100 is completely negligible. Thus in the following we take $p = 100$ and the results are believed to be sufficiently accurate.

Now we investigate the effect of the compliance coefficients on the lowest natural frequency. The results are given in Fig. 3 when the piezoelectric sensor and actuator are both AP. The gradient index is $\kappa = 0.5$, the length-to-inner radius ratio is $L/R = 4$, and the wave numbers are $m = 1$ and $n = 1$.

From Fig. 3, we can find that Ω decreases with \bar{R}_z and \bar{R}_θ , which indicates that the increase of

Table 3 Convergence study of the present method

Total number of fictitious layers p	$L/R = 3$		$L/R = 10$	
	The first order	The fifth order	The first order	The fifth order
90	3.1025618	5.4795977	0.9495751	4.1482559
100	3.1025620	5.4795977	0.9495767	4.1482489

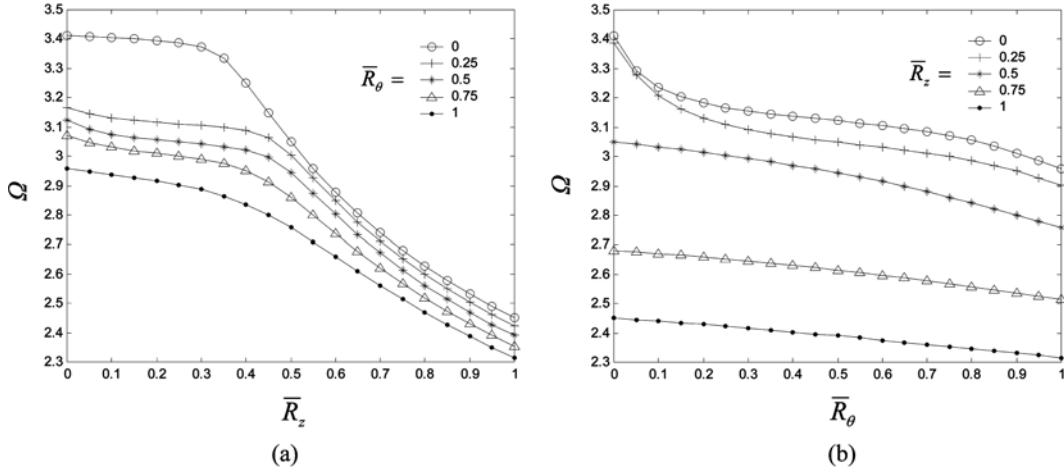


Fig. 3 Effect of imperfect interfaces on the natural frequency (a) Curves of Ω versus \bar{R}_z , (b) Curves of Ω versus \bar{R}_θ

the compliance coefficients will reduce the overall stiffness of the hollow cylinder. The details of reduction however are different in Fig. 3(a) and 3(b). Fig. 3(a) shows that Ω decreases very slowly with \bar{R}_z at the initial stage (about $\bar{R}_z \leq 0.3$), but for larger \bar{R}_z , Ω decreases very quickly. While as shown in Fig. 3(b), Ω decreases very quickly at first stage and then keeps slowly down with \bar{R}_θ as \bar{R}_z is small (i.e., $\bar{R}_z = 0$ and 0.25). In fact, we can observe that the influence of the compliance coefficient \bar{R}_θ on the natural frequency Ω is more significant than that of the compliance coefficient \bar{R}_z at the initial stage. For example, when \bar{R}_θ remains as 0.25 and \bar{R}_z increases from 0 to 0.3, Ω decreases from 3.167 to 3.104 correspondingly, the percentage variation is only 2.0%, which, however, is 8.7% in the case of $\bar{R}_z = 0.25$ and \bar{R}_θ increases from 0 to 0.3, where Ω decreases from 3.388 to 3.092 correspondingly.

Next the effect of compliance coefficients on the mode shape of free vibration is studied. Fig. 4 display the thickness modes of the first and fourth orders. The parameters are taken as $\kappa = 0.2$, $L/R = 5$, $m = 1$ and $n = 2$, and the piezoelectric sensor and actuator are RP and AP, respectively.

From the figure, some conclusions can be drawn. Firstly, when imperfection is involved, the mechanical displacements \bar{u}_θ and \bar{u}_z become discontinuous at the interfaces. Secondly, the appearance of the interfacial bonding imperfection will lead to the re-distribution of stresses. For example, when the interfaces become imperfect, the interfacial normal stress $\bar{\sigma}_{rr}$ at $\eta = 1.75$ (i.e., at the outer interface) increases, while those at $\eta = 1.25$ (i.e., at the inner interface) and at $\eta = 1.5$ (i.e., at the middle surface of the cylinder) decrease, as shown in Fig. 4(a). But the situation may change for different modes. For example, $\bar{\sigma}_{rr}$ at any position decreases once the interfaces become imperfect, as shown in Fig. 4(b). So the effect of weak interfaces on the modes of free vibration may change with parameters such as the order of mode. Thirdly, the interfacial imperfection also has certain effect on the electric field. It can be seen from Fig. 4 that the dimensionless electric potential $\bar{\Phi}$ and the dimensionless electric displacements \bar{D}_r and \bar{D}_θ change with the compliance coefficients obviously. An interesting phenomenon observed from Fig. 4(b) is that the electric displacements \bar{D}_r and \bar{D}_θ in the inner piezoelectric sensor almost vanish once the interface becomes imperfect. Such a character may be utilized to detect interfacial damages in smart structures.

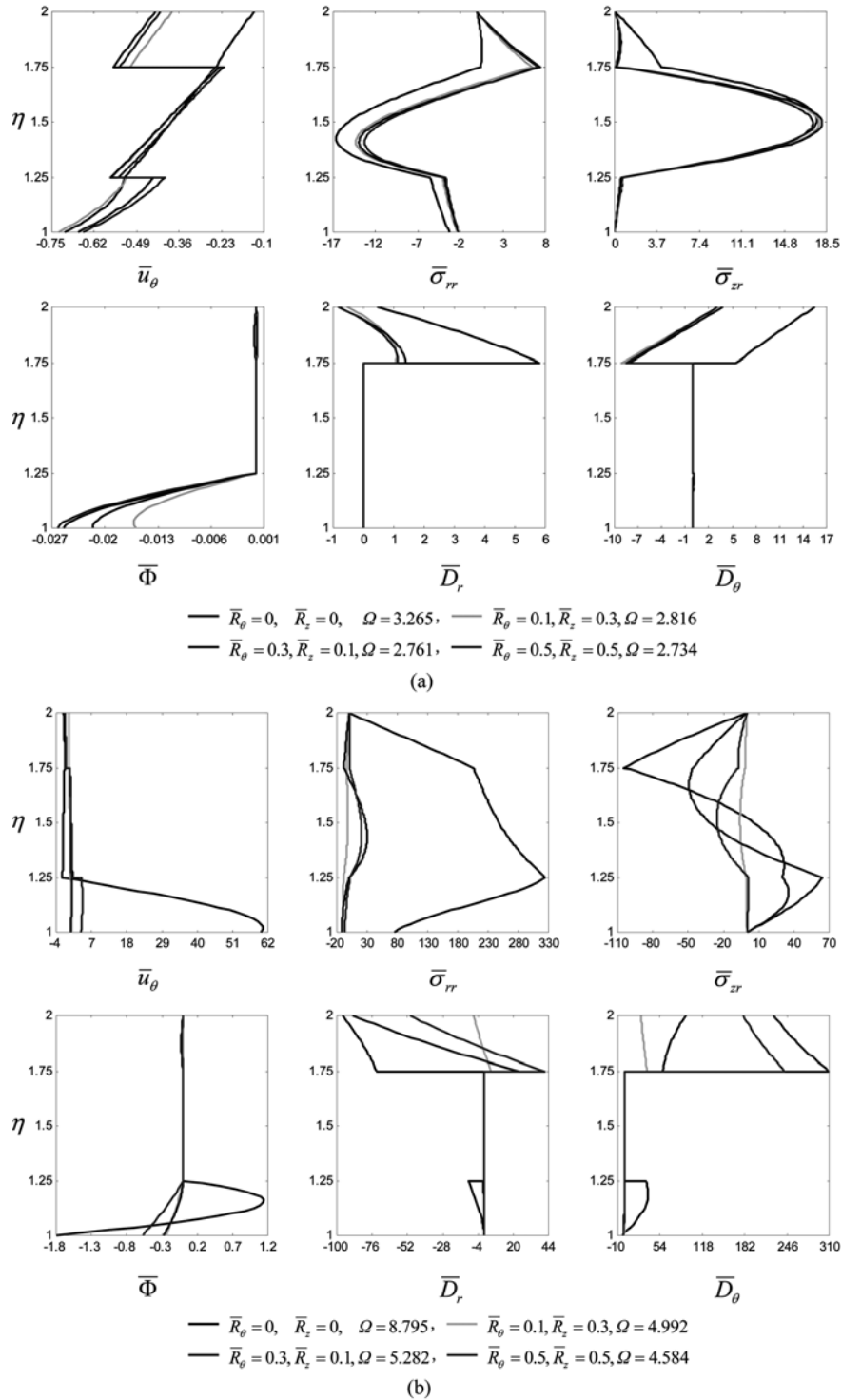


Fig. 4 Distributions of physical variables along the thickness for the thickness mode (a) The first order, (b) The fourth order

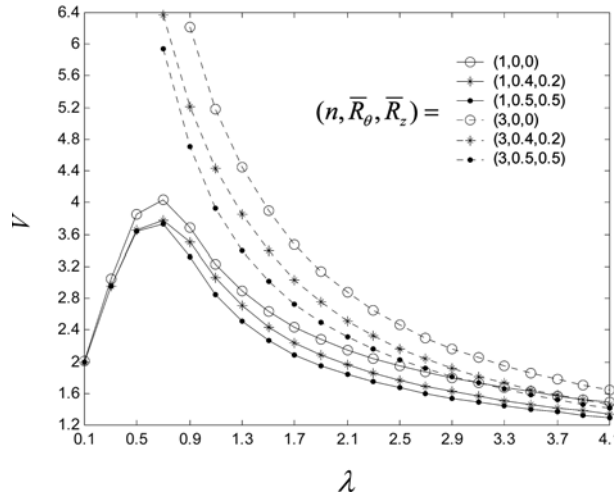


Fig. 5 Dispersion curves for different compliance coefficients

Fig. 5 displays the dispersion curves of the non-dimensional wave phase velocity $V (= \Omega/\lambda)$ versus the non-dimensional axial wave number λ . In this example, we assume $\kappa=1$ and that the piezoelectric sensor and actuator are both RP. Unlike the curves for $n=3$, which descend with λ , the curves for $n=1$ gradually ascend at the beginning, and then they fall down after the peak. This clearly illustrates that the dispersion curves are quite different for different modes. The compliance coefficients also have certain effect on the dispersion curves. In particular, the imperfect interface tends to sink the dispersion curves. However, the effect becomes less significant for larger λ , as can be seen from Fig. 5.

5.3 Steady-state response

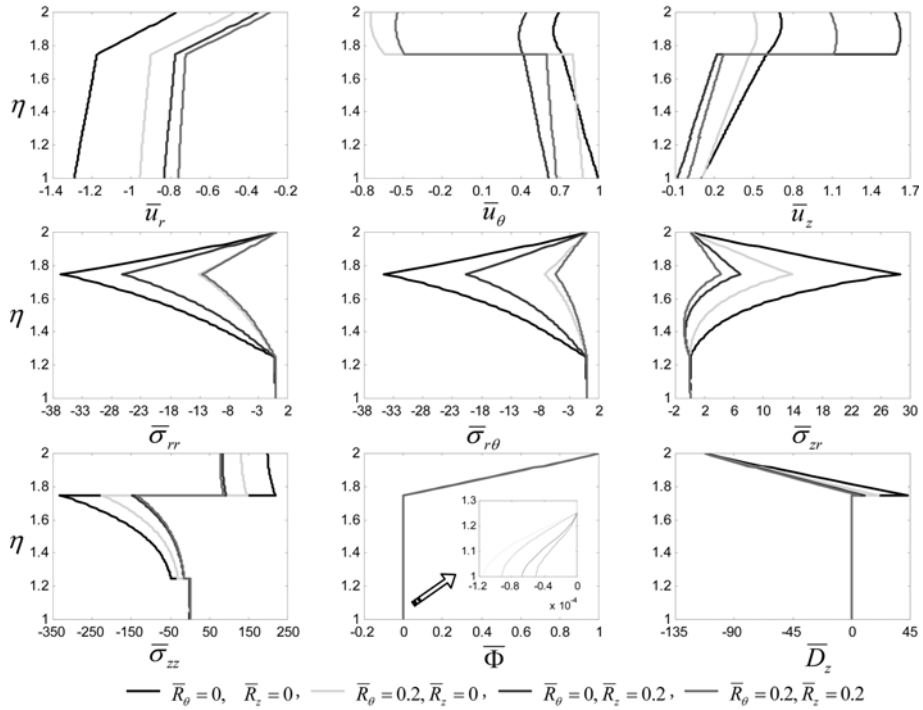
To investigate the steady-state response, the electric potentials applied to the piezoelectric actuator are taken as $\Phi = 0$ at $\eta = \eta_2$ and $\Phi = R\sqrt{c_{44}^s/\chi_{33}^s}\sin(\pi\zeta + \varphi_0)\cos\theta \cdot \exp(i\omega t)$ at $\eta = \eta_3$, respectively. In the following, the dimensionless forcing frequency is $\Omega = 0$ (static bending) or $\Omega = 2$ (forced vibration), and wave numbers are $m = n = 1$.

We first suppose that the piezoelectric sensor and actuator are AP and RP respectively. Meanwhile, we take $L/R = 6$ and $\kappa = 2$. The first two lowest natural frequencies of the smart hollow cylinder with different compliance coefficients are listed in Table 4.

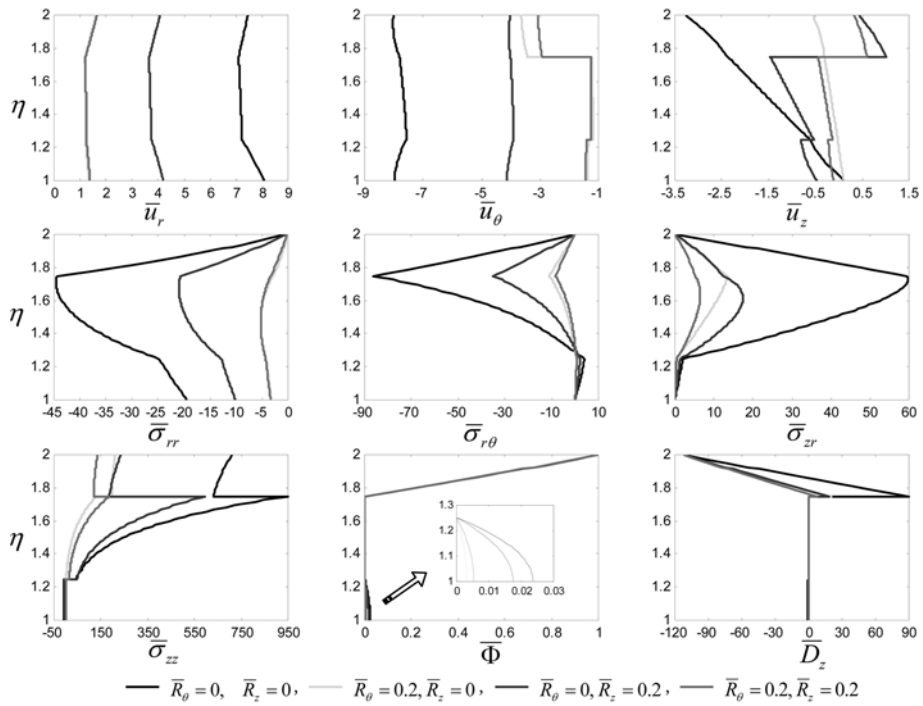
Fig. 6 displays the effect of weak interfaces on the steady-state response, from which we can find that the mechanical displacement \bar{u}_r is continuous in the radial direction, since only slip-type weak

Table 4 The first two lowest natural frequencies for different compliance coefficients

Ω	$(\bar{R}_\theta, \bar{R}_z)$			
	(0,0)	(0.2,0)	(0,0.2)	(0.2,0.2)
The first order	1.8825	1.8009	1.8469	1.7985
The second order	4.1911	4.0685	3.9699	3.6463



(a)



(b)

Fig. 6 Effect of bonding imperfection on the steady-state response (a) $\Omega = 0$ (static bending), (b) $\Omega = 2$

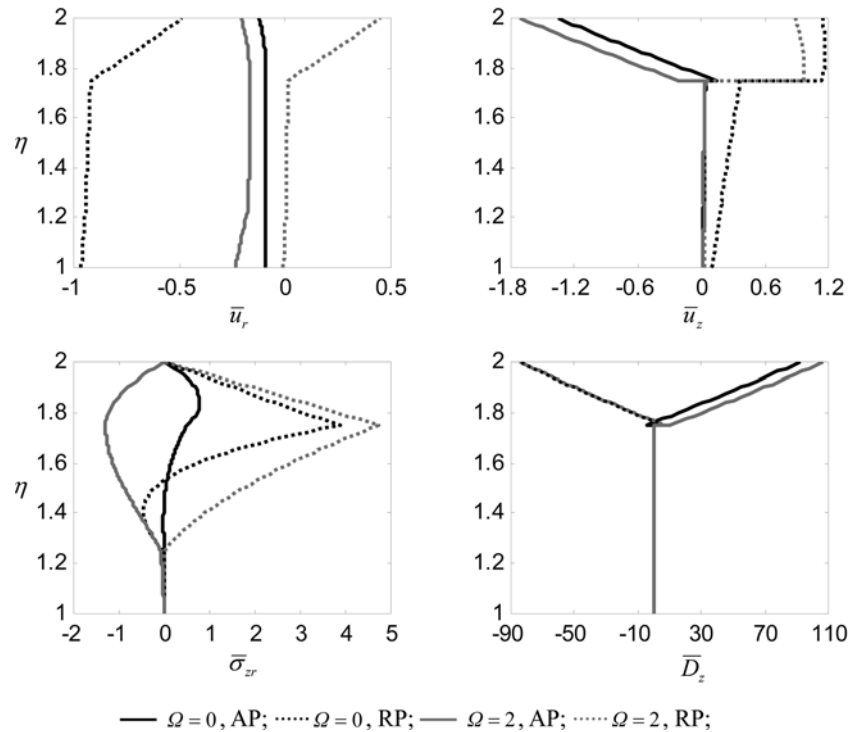


Fig. 7 Effect of direction of polarization on the steady-state response

bonding at interfaces is considered. Analogously, the mechanical displacements \bar{u}_z (or \bar{u}_θ) are also continuous at the interfaces if the compliance coefficient \bar{R}_z (or \bar{R}_θ) is taken to be zero. The stress $\bar{\sigma}_{zz}$ is discontinuous at the interfaces because of the difference of elastic moduli between the elastic FG layer and piezoelectric layers.

Bian *et al.* (2006a, b) showed that the mechanical displacement will increase with the compliance coefficients of the weak interfaces for a smart beam subjected to a mechanical load. When only an electric load is applied on the piezoelectric actuator as considered in this example, almost all mechanical and electrical quantities decrease with the compliance coefficients, as shown in Fig. 6. Hence, the steady-state response of a smart structure can be adjusted not only by changing the applied voltage but also by controlling the bonding condition of the interfaces.

The effect of direction of polarization of a piezoelectric actuator on the response of the smart hollow cylinder is shown in Fig. 7, where the parameters are chosen as $L/R = 8$, $\kappa = 1$ and $\bar{R}_\theta = \bar{R}_z = 0.2$. The piezoelectric sensor is supposed to be RP.

As shown in Fig. 7, the static radial displacement \bar{u}_r ($\Omega = 0$) for the AP piezoelectric actuator is smaller than that for the RP one, while the dynamic radial displacement ($\Omega = 2$) for the AP piezoelectric actuator is larger than that for the RP one. When the direction of polarization alters from AP to RP, both the slip displacement \bar{u}_z and the interfacial shear stress $\bar{\sigma}_{zr}$, at the outer interface increases. The electric displacement \bar{D}_z in the actuator even changes from positive values to negative values. All these observations indicate that both the mechanical and electrical quantities are affected by the direction of polarization of the piezoelectric actuator significantly. This characteristic may be useful in obtaining an optimum actuating function for a practical smart structure.

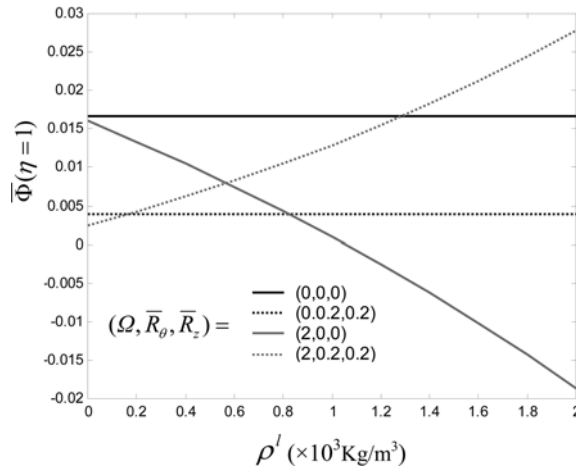


Fig. 8 Variation of the electric potential of sensor with the fluid density

Finally the effect of the fluid parameters on the response of the hybrid cylinder is discussed. Fig. 8 displays curves of the electric potential at the sensor's inner surface ($\bar{\Phi}(\eta=1)$) versus the density of the filled fluid, where $L/R=10$, $\kappa=0.5$ and both the piezoelectric sensor and actuator are RP.

For the static bending ($\Omega=0$), it is interesting that the electric potential of the sensor maintains invariable as the fluid density increases, whether the interfaces are perfect or imperfect. The electric potential, however, depends greatly on the fluid density when the cylinder is applied a dynamic motivation (e.g., $\Omega=2$). It decreases with the fluid density if the interfaces are perfect ($\bar{R}_\theta = \bar{R}_z = 0$), while it increases as the interfaces become imperfect (e.g. $\bar{R}_\theta = \bar{R}_z = 0.2$). In a word, this characteristic of the smart cylinder may be applied in practice, such as identifying the kind of the fluid filled in the cylinder, etc.

6. Conclusions

This paper presents a three-dimensional analysis of the coupled free vibration and steady-state response of a smart hollow cylinder, which is fully filled with a non-viscous, compressible fluid medium and simultaneously embedded in an elastic medium. To describe the possible weakness of interfaces between the homogeneous piezoelectric actuator/sensor and the elastic FG material, a general linear spring-layer model is employed, which is suitable at least at the initial stage of the interfacial debonding. The analysis is rather straightforward and very effective as state space formulations have been employed. No assumption on the distribution along the radial direction of any mechanical or electric field variable is introduced, and hence the results obtain in this paper can serve as benchmarks for clarifying the simplified theories and numerical methods.

As shown in the numerical examples, the presence of the weak interfaces will decrease the natural frequencies, which indicates the reduction of global stiffness of the smart hollow cylinder. The degree of such effect, however, is different on different physical quantities and for different parameters. In the smart cylinder, the interfacial imperfection will lead to not only the re-distribution of the mechanical field, but also the re-distribution of the electric field. Since the weak interfaces

decrease the interaction between the host structure and the actuator/sensor, the amplitude of the steady-state response induced by the actuator will be reduced if the interfaces become imperfect. This is different from that of the smart cylinder subjected to a single mechanical loading. It is also shown that the direction of polarization of the piezoelectric actuator has an obvious effect on the response of the smart hollow cylinder, which enlightens us on an alternative way to control or design smart structures. The relationship between the electric potential of the sensor and the density of the filled fluid is studied finally, and an application of the smart cylinder is discussed.

Acknowledgements

The work was supported by the National Natural Science Foundation of China (No. 10432030, 10725210 and 10702061), the Research Foundation for Scholars of NIT (No. 1142357G608), the Specialized Research Fund for the Doctoral Program of Higher Education (No. 20060335107) and the Program for New Century Excellent Talents in University (No. NCET-05-05010).

References

- Aboudi, J. (1987), "Damage in composites-modeling of imperfect bonding", *Compos. Sci. Technol.*, **28**, 103-128.
- Achenbach, J.D. and Zhu, H. (1989), "Effect of interracial zone on mechanical behaviour and failure of fibre-reinforced composites", *J. Mech. Phys. Solids*, **37**, 381-393.
- Benveniste, Y. (1985), "The effective mechanical behaviour of composite materials with imperfect contact between the constituents", *Mech. Mater.*, **4**, 197-208.
- Bian, Z.G., Ying, J., Chen, W.Q. and Ding, H.J. (2006a), "Bending and free vibration analysis of a smart functionally graded plate", *Struct. Eng. Mech.*, **23**, 97-113.
- Bian, Z.G., Lim, C.W. and Chen, W.Q. (2006b), "On functionally graded beams with integrated surface piezoelectric layers", *Compos. Struct.*, **72**, 339-351.
- Botta, F. and Cerri, G. (2007), "Wave propagation in Reissner-Mindlin piezoelectric coupled cylinder with non-constant electric field through the thickness", *Int. J. Solid. Struct.*, **44**, 6201-6219.
- Chen, W.Q., Bian, Z.G., Lv, C.F. and Ding, H.J. (2004a), "3D free vibration analysis of a functionally graded piezoelectric hollow cylinder filled with compressible fluid", *Int. J. Solid. Struct.*, **41**, 947-964.
- Chen, W.Q., Cai, J.B. and Ye, G.R. (2003), "Exact solutions of cross-ply laminate with bonding imperfections", *AIAA J.*, **41**, 2244-2250.
- Chen, W.Q. and Lee, K.Y. (2004), "Three-dimensional exact analysis of angle-ply laminates in cylindrical bending with interfacial damage via state space method", *Compos. Struct.*, **64**, 275-283.
- Chen, W.Q., Ying, J., Cai, J.B. and Ye, G.R. (2004b), "Benchmark solution of laminated beams with bonding imperfections", *AIAA J.*, **42**, 426-429.
- Chen, W.Q., Wang, Y.F., Cai, J.B. and Ye, G.R. (2004c), "Three-dimensional analysis of cross-ply laminated cylindrical panels with weak interfaces", *Int. J. Solid. Struct.*, **41**, 2429-2446.
- Chen, W.Q., Jung, J.P. and Lee, K.Y. (2006), "Static and dynamic behavior of simply-supported cross-ply laminated piezoelectric cylindrical panels with imperfect bonding", *Compos. Struct.*, **74**, 265-276.
- Cheng, Z.Q., Jemah, A.K. and Williams, F.W. (1996), "Theory of multilayered anisotropic plates with weakened interfaces", *J. Appl. Mech.*, **63**, 1019-1026.
- Crawley, E.F. and Luis, J.D. (1987), "Use of piezoelectric actuators as elements of intelligent structures", *AIAA J.*, **25**, 1373-1385.
- Della, C.N. and Shu, D.W. (2007), "Free vibration analysis of delaminated bimaterial beams", *Compos. Struct.*, **80**, 212-220.
- Ding, H.J. and Chen, W.Q. (2001), *Three Dimensional Problems of Piezoelectricity*, Nova Science Publishers,

- New York, USA.
- Dollar, A. and Steif, P.S. (1988), "Load transfer in composites with a Coulumb friction interface", *Int. J. Solid Struct.*, **24**, 789-803.
- Galassi, C., Dinescu, M., Uchino, K. and Sayer, M. (2000), *Piezoelectric Materials: Advances in Science, Technology and Applications*, Kluwer Academic Publisher, Boston/Dordrecht, USA/The Netherlands.
- Gorokhovskya, V., Bowmana, C., Gannon, P., VanVorousa, D., Voevodinb, A.A., Rutkowskib, A., Muratorec, C., Smithd, R.J., Kayanid, A., Gellese, D., Shutthanandane, V. and Trusov, B.G. (2006), "Tribological performance of hybrid filtered arc-magnetron coatings: Part I: Coating deposition process and basic coating properties characterization", *Surf. Coat. Tech.*, **201**, 3732-3747.
- Gorokhovskya, V., Bowman, C., Gannon, P., VanVorous, D., Voevodin, A.A. and Rutkowski, A. (2007), "Tribological performance of hybrid filtered arc-magnetron coatings Part II: Tribological properties characterization", *Surf. Coat. Tech.*, **201**, 6228-6238.
- Haddadpour, H., Mahmoudkhani, S. and Navazi, H.M. (2007), "Free vibration analysis of functionally graded cylindrical shells including thermal effects", *Thin Wall. Struct.*, **45**, 591-599.
- Hashin, Z. (1990), "Thermoelastic properties of fibre composites with imperfect interface", *Mech. Mater.*, **8**, 333-348.
- Hashin, Z. (1991a), "Thermoelastic properties of particulate composites with imperfect interface", *J. Mech. Phys. Solids*, **39**, 745-762.
- Hashin, Z. (1991b), "The Spherical inclusion with imperfect interface", *J. Appl. Mech.*, **58**, 444-449.
- He, L.H. and Lim, C.W. (2003), "Electromechanical responses of piezoelectric fiber composites with sliding interface under anti-plane deformations", *Compos. Part B-Eng.*, **34**, 373-381.
- Huang, X.L. and Shen, H.S. (2006), "Vibration and dynamic response of functionally graded plates with piezoelectric actuators in thermal environments", *J. Sound Vib.*, **289**, 25-53.
- Junger, M.C. and Feit, D. (1993), *Sound Structures, and Their Interaction*, Acoustical Society of America, Woodbury, USA.
- Kapuria, S., Bhattacharyya, M. and Kumar, A.N. (2006), "Assessment of coupled 1D models for hybrid piezoelectric layered functionally graded beams", *Compos. Struct.*, **72**, 455-468.
- Librescu, L. and Schmidt, R. (2001), "A general linear theory of laminated composite shells featuring interlaminar bonding imperfections", *Int. J. Solid Struct.*, **38**, 3355-3375.
- Ling, Y.H., Li, J.T., Ge, C.C. and Bai, X.D. (2002), "Fabrication and evaluation of SiC/Cu functionally graded material used for plasma facing components in a fusion reactor", *J. Nucl. Mater.*, **303**, 188-195.
- Lipton, R. (2001), "Effect of interfacial bonding on fiber reinforced shafts subject to antiplane shear", *Int. J. Solid Struct.*, **38**, 369-387.
- Mahmoud, N.A. (2003), "Reduction of thermal stresses by developing two-dimensional functionally graded materials", *Int. J. Solid Struct.*, **40**, 7339-7356.
- Moore, I.D. (2001), "Buried pipes and culverts", *Geotech. Geoenviron. Eng. Handb.*, **18**, 541-567.
- Pagano, N.J. and Tandon, G.P. (1990), "Modeling of imperfect bonding in fiber reinforced brittle matrix composites", *Mech. Mater.*, **9**, 49-64.
- Pompe, W., Worch, H., Epple, M., Friess, W., Gelinsky, M., Greil, P., Hempel, U., Scharnweber, D. and Schulte, K. (2003), "Functionally graded materials for biomedical applications", *Mater. Sci. Eng.*, **362**, 40-60.
- Qu, J.M. (1993a), "Eshelby tensor for an elastic inclusion with slightly weakened interfaces", *J. Appl. Mech.*, **60**, 1048-1050.
- Qu, J.M. (1993b), "The effect of slightly weakened interfaces on the overall elastic properties of composite materials", *Mech. Mater.*, **14**, 269-281.
- Ray, M.C. and Reddy, J.N. (2005), "Active control of laminated cylindrical shells using piezoelectric fiber reinforced composites", *Compos. Sci. Tech.*, **65**, 1226-1236.
- Ray, M.C. and Sachade, H.M. (2006), "Finite element analysis of smart functionally graded plates", *Int. J. Solid Struct.*, **43**, 5468-5484.
- Reddy, J.N. and Cheng, Z.Q. (2001), "Three-dimensional solutions of smart functionally graded plates", *J. Appl. Mech.*, **68**, 234-241.
- Rokhlin, S.I., Wang, L., Xie, B., Yakovlev, V.A. and Adler, L. (2004), "Modulated angle beam ultrasonic spectroscopy for evaluation of imperfect interfaces and adhesive bonds", *Ultrasonics*, **42**, 1037-1047.

- Shakeri, M., Akhlaghi, M. and Hoseini, S.M. (2006), "Vibration and radial wave propagation velocity in functionally graded thick hollow cylinder", *Compos. Struct.*, **76**, 174-181.
- Simões Moita, J.M., Correia, I.F.P., Mota Soares, C.M.M. and Mota Soares, C.A. (2004), "Active control of adaptive laminated structures with bonded piezoelectric sensors and actuators", *Comput. Struct.*, **82**, 1349-1358.
- Sun, D.C., Tong, L.Y. and Atluri, S.N. (2001), "Effects of piezoelectric sensor/actuator debonding on vibration control of smart beams", *Int. J. Solid. Struct.*, **38**, 9033-9051.
- Tan, P. and Tong, L.Y. (2004), "Identification of delamination in a composite beam using integrated piezoelectric sensor/actuator layer", *Compos. Struct.*, **66**, 391-398.
- Tan, P. and Tong, L.Y. (2006), "A sensor charge output deviation method for delamination detection using isolated piezoelectric actuator and sensor patches", *Compos. Part B-Eng.*, **37**, 583-592.
- Tiersten, H.F. (1969), *Linear Piezoelectric Plate Vibration*, Plenum Press, New York, USA.
- Tzou, H.S. and Anderson, G.L. (1992), *Intelligent Structural Systems*, Kluwer Academic Publisher, Boston/Dordrecht, USA/The Netherlands.
- Tzou, H.S. (1993), *Piezoelectric Shells, Distributed Sensing and Control of Continua*, Kluwer Academic Publisher, Boston/Dordrecht, USA/The Netherlands.
- Wilson, S.A., Jourdain, R.P.J., Zhanga, Q., Doreya, R.A., Bowen, C.R., Willanderc, M., Wahabd, O.U., Willandere, M., Al-hillie, S.M., Nure, O., Quandtf, E., Johansson, C., Pagounish, E., Kohli, M., Matovicj, J., Samelk, B., Van der Wijngaartk, W., Jagerl, E.W.J., Carlssonl, D., Djinovicj, Z., Wegenerp, M., Moldovanm, C., Iosubm, R., Abadn, E., Wendlandto, M., Rusug, C. and Persson, K. (2007), "New materials for micro-scale sensors and actuators: An engineering review", *Mater. Sci. Eng. R. Rep.*, **56**, 1-129.
- Zhong, F.H. and Folias, E.S. (1992), "The 3D stress field of a fiber embedded into a matrix and subjected to an axial load", *Comput. Mech.*, **9**, 233-247.

Appendix

1. AP

For AP, the matrix \mathbf{M} in Eq. (4) is

$$\mathbf{M} = \begin{bmatrix} \mathbf{M}_{11} & \mathbf{M}_{12} \\ \mathbf{M}_{21} & \mathbf{M}_{22} \end{bmatrix}$$

$$\mathbf{M}_{11} = \begin{bmatrix} 0 & 0 & 0 & \frac{e_{15}}{\alpha} \\ 0 & \frac{1}{r} & 0 & 0 \\ \frac{k_2}{r} \frac{\partial}{\partial z} & \frac{k_1}{r^2} \frac{\partial}{\partial \theta} & \left(\frac{c_{12}}{c_{11}} - 1\right) \frac{1}{r} & 0 \\ -\frac{e_{24}}{r^2} \frac{\partial^2}{\partial \theta^2} - k_5 \frac{\partial^2}{\partial z^2} & -\frac{e_{24} + k_3}{r} \frac{\partial^2}{\partial \theta \partial z} & -\frac{e_{31}}{c_{11}} \frac{\partial}{\partial z} & -\frac{1}{r} \end{bmatrix}$$

$$\mathbf{M}_{12} = \begin{bmatrix} \frac{\chi_{11}}{\alpha} & 0 & -\frac{\partial}{\partial z} & 0 \\ 0 & \frac{1}{c_{66}} & -\frac{1}{r} \frac{\partial}{\partial \theta} & 0 \\ -\frac{\partial}{\partial z} & -\frac{1}{r} \frac{\partial}{\partial \theta} & \rho \frac{\partial^2}{\partial t^2} + \frac{k_1}{r^2} & \frac{k_3}{r} \frac{\partial}{\partial z} \\ 0 & 0 & -\frac{k_3}{r} \frac{\partial}{\partial z} & \frac{\chi_{22}}{r^2} \frac{\partial^2}{\partial \theta^2} + k_6 \frac{\partial^2}{\partial z^2} \end{bmatrix}$$

(A1-1)

$$\mathbf{M}_{21} = \begin{bmatrix} \rho \frac{\partial^2}{\partial t^2} - \frac{c_{44}}{r^2} \frac{\partial^2}{\partial \theta^2} - k_4 \frac{\partial^2}{\partial z^2} & -\frac{c_{44} + k_2}{r} \frac{\partial^2}{\partial \theta \partial z} & -\frac{c_{13}}{c_{11}} \frac{\partial}{\partial z} & 0 \\ -\frac{c_{44} + k_2}{r} \frac{\partial^2}{\partial \theta \partial z} & \rho \frac{\partial^2}{\partial t^2} - \frac{k_1}{r^2} \frac{\partial^2}{\partial \theta^2} - c_{44} \frac{\partial^2}{\partial z^2} & -\frac{c_{12}}{c_{11}} \frac{1}{r} \frac{\partial}{\partial \theta} & 0 \\ -\frac{c_{13}}{c_{11}} \frac{\partial}{\partial z} & -\frac{c_{12}}{c_{11}} \frac{1}{r} \frac{\partial}{\partial \theta} & \frac{1}{c_{11}} & 0 \\ 0 & 0 & 0 & -\frac{c_{55}}{\alpha} \end{bmatrix}$$

$$\mathbf{M}_{22} = \begin{bmatrix} -\frac{1}{r} & 0 & -\frac{k_2}{r} \frac{\partial}{\partial z} & -\frac{e_{24}}{r^2} \frac{\partial^2}{\partial \theta^2} - k_5 \frac{\partial^2}{\partial z^2} \\ 0 & -\frac{2}{r} & -\frac{k_1}{r^2} \frac{\partial}{\partial \theta} & -\frac{e_{24} + k_3}{r} \frac{\partial^2}{\partial \theta \partial z} \\ 0 & 0 & -\frac{c_{12}}{c_{11}} \frac{1}{r} & -\frac{e_{31}}{c_{11}} \frac{\partial}{\partial z} \\ \frac{e_{15}}{\alpha} & 0 & 0 & 0 \end{bmatrix}$$

The matrix **N** in Eq. (5) is

$$\mathbf{N} = \begin{bmatrix} k_4 \frac{\partial}{\partial z} & \frac{k_2}{r} \frac{\partial}{\partial \theta} & \frac{c_{13}}{c_{11}} & 0 & 0 & 0 & \frac{k_2}{r} & k_5 \frac{\partial}{\partial z} \\ k_2 \frac{\partial}{\partial z} & \frac{k_1}{r} \frac{\partial}{\partial \theta} & \frac{c_{12}}{c_{11}} & 0 & 0 & 0 & \frac{k_1}{r} & k_3 \frac{\partial}{\partial z} \\ \frac{c_{44}}{r} \frac{\partial}{\partial \theta} & c_{44} \frac{\partial}{\partial z} & 0 & 0 & 0 & 0 & 0 & \frac{e_{24}}{r} \frac{\partial}{\partial \theta} \\ k_5 \frac{\partial}{\partial z} & \frac{k_3}{r} \frac{\partial}{\partial \theta} & \frac{e_{31}}{c_{11}} & 0 & 0 & 0 & \frac{k_3}{r} & -k_6 \frac{\partial}{\partial z} \\ \frac{e_{24}}{r} \frac{\partial}{\partial \theta} & e_{24} \frac{\partial}{\partial z} & 0 & 0 & 0 & 0 & 0 & -\frac{\varepsilon_{22}}{r} \frac{\partial}{\partial \theta} \end{bmatrix} \quad (\text{A1-2})$$

The matrix **D** in Eq. (9) is

$$\mathbf{D} = \begin{bmatrix} \mathbf{D}_{11} & \mathbf{D}_{12} \\ \mathbf{D}_{21} & \mathbf{D}_{22} \end{bmatrix}$$

$$\mathbf{D}_{11} = \begin{bmatrix} 0 & 0 & 0 & \frac{e_{15}}{\alpha} \sqrt{c_{44}^s \chi_{33}^s} \\ 0 & \frac{1}{\eta} & 0 & 0 \\ -\frac{k_2}{c_{44}^1} \frac{\lambda}{\eta} & \frac{k_1}{c_{44}^1} \frac{n}{\eta^2} & \frac{(c_{12} - 1)}{c_{11}} \frac{1}{\eta} & 0 \\ \frac{e_{24}}{\sqrt{c_{44}^s \chi_{33}^s}} \left(\frac{n}{\eta}\right)^2 + \frac{k_5}{\sqrt{c_{44}^s \chi_{33}^s}} \lambda^2 & -\lambda \frac{e_{24} + k_3}{\sqrt{c_{44}^s \chi_{33}^s}} \frac{n}{\eta} & -\lambda \frac{e_{31}}{c_{11}} \sqrt{\frac{c_{44}^s}{\chi_{33}^s}} & -\frac{1}{\eta} \end{bmatrix} \quad (\text{A1-3})$$

$$\mathbf{D}_{12} = \begin{bmatrix} \frac{\varepsilon_{11}}{\alpha} c_{44}^s & 0 & -\lambda & 0 \\ 0 & \frac{c_{44}^s}{c_{66}} & \frac{n}{\eta} & 0 \\ \lambda & -\frac{n}{\eta} & \frac{k_1}{\eta^2} \frac{1}{c_{44}^s} - \frac{\rho}{\rho^s} \Omega^2 & -\frac{k_3}{\eta} \frac{1}{\sqrt{c_{44}^s \chi_{33}^s}} \lambda \\ 0 & 0 & -\frac{k_3}{\eta} \frac{1}{\sqrt{c_{44}^s \chi_{33}^s}} \lambda & -\frac{\varepsilon_{22}}{\varepsilon_{33}^s} \frac{n^2}{\eta^2} - \frac{k_6}{\chi_{33}^s} \lambda^2 \end{bmatrix}$$

$$\mathbf{D}_{21} = \begin{bmatrix} \frac{c_{44}}{c_{44}^s} \left(\frac{n}{\eta}\right)^2 + \frac{k_4}{c_{44}^s} \lambda^2 - \frac{\rho}{\rho^s} \Omega^2 & -\frac{c_{44} + k_2}{c_{44}^s} \frac{n}{\eta} \lambda & -\frac{c_{13}}{c_{11}} \lambda & 0 \\ -\frac{c_{44} + k_2}{c_{44}^s} \lambda \frac{n}{\eta} & \frac{k_1}{c_{44}^s} \left(\frac{n}{\eta}\right)^2 + \frac{c_{44}}{c_{44}^s} \lambda^2 - \frac{\rho}{\rho^s} \Omega^2 & \frac{c_{12}}{c_{11}} \frac{n}{\eta} & 0 \\ \frac{c_{13}}{c_{11}} \lambda & -\frac{c_{12}}{c_{11}} \frac{n}{\eta} & \frac{c_{44}^s}{c_{11}} & 0 \\ 0 & 0 & 0 & -\frac{c_{55}}{\alpha} \chi_{33}^s \end{bmatrix}$$

$$\mathbf{D}_{22} = \begin{bmatrix} -\frac{1}{\eta} & 0 & -\frac{k_2 \lambda}{c_{44}^s \eta} & \frac{e_{24}}{\sqrt{c_{44}^s \chi_{33}^s}} \left(\frac{n}{\eta}\right)^2 + \frac{k_5}{\sqrt{c_{44}^s \chi_{33}^s}} \lambda^2 \\ 0 & -\frac{2}{\eta} & \frac{k_1 n}{c_{44}^s \eta^2} & -\frac{e_{24} + k_3}{\sqrt{c_{44}^s \chi_{33}^s}} \frac{n}{\eta} \lambda \\ 0 & 0 & -\frac{c_{12}}{c_{11}} \frac{1}{\eta} & \frac{e_{31}}{c_{11}} \sqrt{\frac{c_{44}^s}{\chi_{33}^s}} \lambda \\ \frac{e_{15}}{\alpha} \sqrt{c_{44}^s \chi_{33}^s} & 0 & 0 & 0 \end{bmatrix}$$

where ρ^s is the mass density of the piezoelectric sensor, and

$$\begin{aligned} k_1 &= c_{22} - c_{12}^2 / c_{11}, \quad k_2 = c_{23} - c_{12} c_{13} / c_{11}, \quad k_3 = e_{32} - c_{12} e_{31} / c_{11}, \quad k_4 = c_{33} - c_{13}^2 / c_{11} \\ k_5 &= e_{33} - c_{13} e_{31} / c_{11}, \quad k_6 = \chi_{33} + e_{31}^2 / c_{11}, \quad \alpha = c_{55} \chi_{11} + e_{15}^2, \quad \lambda = m\pi R / L, \quad \Omega = \omega R \sqrt{\rho^s / c_{44}^s} \end{aligned} \quad (\text{A1-4})$$

2. RP

For RP, the matrix \mathbf{M} in Eq. (4) is

$$\mathbf{M} = \begin{bmatrix} \mathbf{M}_{11} & \mathbf{M}_{12} \\ \mathbf{M}_{21} & \mathbf{M}_{22} \end{bmatrix}$$

$$\mathbf{M}_{11} = \begin{bmatrix} 0 & 0 & 0 & 0 \\ 0 & \frac{1}{r} & 0 & 0 \\ \frac{k_3}{r} \frac{\partial}{\partial z} & \frac{k_1}{r^2} \frac{\partial}{\partial \theta} & \frac{\beta_1 - 1}{r} & \frac{\gamma_1}{r} \\ 0 & 0 & 0 & -\frac{1}{r} \end{bmatrix}$$

$$\mathbf{M}_{12} = \begin{bmatrix} \frac{1}{c_{44}} & 0 & -\frac{\partial}{\partial z} & -\frac{e_{24}}{c_{44}} \frac{\partial}{\partial z} \\ 0 & \frac{1}{c_{55}} & -\frac{\partial}{r \partial \theta} & -\frac{e_{15}}{c_{55}} \frac{\partial}{r \partial \theta} \\ -\frac{\partial}{\partial z} & -\frac{\partial}{r \partial \theta} & \rho \frac{\partial^2}{\partial t^2} + \frac{k_1}{r^2} & 0 \\ -\frac{e_{24}}{c_{44}} \frac{\partial}{\partial z} & -\frac{e_{15}}{c_{55}} \frac{\partial}{r \partial \theta} & 0 & k_5 \frac{\partial^2}{r^2 \partial \theta^2} + k_6 \frac{\partial^2}{\partial z^2} \end{bmatrix} \quad (\text{A2-1})$$

$$\mathbf{M}_{21} = \begin{bmatrix} \rho \frac{\partial^2}{\partial t^2} - c_{66} \frac{\partial^2}{r^2 \partial \theta^2} - k_4 \frac{\partial^2}{\partial z^2} & -\frac{k_2 + c_{66}}{r} \frac{\partial^2}{\partial \theta \partial z} & -\beta_2 \frac{\partial}{\partial z} & -\gamma_2 \frac{\partial}{\partial z} \\ -\frac{k_3 + c_{66}}{r} \frac{\partial^2}{\partial \theta \partial z} & \rho \frac{\partial^2}{\partial t^2} - k_1 \frac{\partial^2}{r^2 \partial \theta^2} - c_{66} \frac{\partial^2}{\partial z^2} & -\frac{\beta_1}{r} \frac{\partial}{\partial \theta} & -\frac{\gamma_1}{r} \frac{\partial}{\partial \theta} \\ -\beta_2 \frac{\partial}{\partial z} & -\frac{\beta_1}{r} \frac{\partial}{\partial \theta} & \frac{\chi_{33}}{\alpha} & \frac{e_{33}}{\alpha} \\ -\gamma_2 \frac{\partial}{\partial z} & -\frac{\gamma_1}{r} \frac{\partial}{\partial \theta} & \frac{e_{33}}{\alpha} & \frac{c_{33}}{\alpha} \end{bmatrix}$$

$$\mathbf{M}_{22} = \begin{bmatrix} -\frac{1}{r} & 0 & -\frac{k_2}{r} \frac{\partial}{\partial z} & 0 \\ 0 & -\frac{2}{r} & -\frac{k_1}{r^2} \frac{\partial}{\partial \theta} & 0 \\ 0 & 0 & -\frac{\beta_1}{r} & 0 \\ 0 & 0 & -\frac{\gamma_1}{r} & 0 \end{bmatrix}$$

The matrix **N** in Eq. (5) is

$$\mathbf{N} = \begin{bmatrix} k_4 \frac{\partial}{\partial z} & \frac{k_2}{r} \frac{\partial}{\partial \theta} & \beta_2 & \gamma_2 & 0 & 0 & \frac{k_2}{r} & 0 \\ k_3 \frac{\partial}{\partial z} & \frac{k_1}{r} \frac{\partial}{\partial \theta} & \beta_1 & \gamma_1 & 0 & 0 & \frac{k_1}{r} & 0 \\ \frac{c_{66}}{r} \frac{\partial}{\partial \theta} & c_{66} \frac{\partial}{\partial z} & 0 & 0 & 0 & 0 & 0 & 0 \\ 0 & 0 & 0 & 0 & \frac{e_{24}}{c_{44}} & 0 & 0 & -k_6 \frac{\partial}{\partial z} \\ 0 & 0 & 0 & 0 & 0 & \frac{e_{15}}{c_{55}} & 0 & -\frac{k_5}{r} \frac{\partial}{\partial \theta} \end{bmatrix} \tag{A2-2}$$

The matrix **D** in Eq. (9) is

$$\mathbf{D} = \begin{bmatrix} \mathbf{D}_{11} & \mathbf{D}_{12} \\ \mathbf{D}_{21} & \mathbf{D}_{22} \end{bmatrix}$$

$$\mathbf{D}_{11} = \begin{bmatrix} 0 & 0 & 0 & 0 \\ 0 & \frac{1}{\eta} & 0 & 0 \\ -\frac{k_3}{c_{44}^s} \frac{\lambda}{\eta} & \frac{k_1}{c_{44}^s} \frac{n}{\eta^2} & \frac{\beta_1 - 1}{\eta} & \frac{\gamma_1}{\eta} \sqrt{\frac{\chi_{33}^s}{c_{44}^s}} \\ 0 & 0 & 0 & -\frac{1}{\eta} \end{bmatrix}$$

$$\mathbf{D}_{12} = \begin{bmatrix} \frac{c_{44}^s}{c_{44}} & 0 & -\lambda & -\lambda \frac{e_{24}}{c_{44}} \sqrt{\frac{c_{44}^s}{\chi_{33}^s}} \\ 0 & \frac{c_{44}^s}{c_{55}} & \frac{n}{\eta} & \frac{e_{15}}{c_{55}} \sqrt{\frac{c_{44}^s}{\chi_{33}^s}} \frac{n}{\eta} \\ \lambda & -\frac{n}{\eta} & \frac{k_1}{c_{44}^s} \frac{1}{\eta^2} - \frac{\rho}{\rho^s} \Omega^2 & 0 \\ \lambda \frac{e_{24}}{c_{44}} \sqrt{\frac{c_{44}^s}{\chi_{33}^s}} & -\frac{e_{15}}{c_{55}} \sqrt{\frac{c_{44}^s}{\chi_{33}^s}} \frac{n}{\eta} & 0 & -\frac{k_5}{\chi_{33}^s} \left(\frac{n}{\eta}\right)^2 - \frac{k_6}{\chi_{33}^s} \lambda^2 \end{bmatrix} \tag{A2-3}$$

$$\mathbf{D}_{21} = \begin{bmatrix} \frac{c_{66}}{c_{44}^s} \left(\frac{n}{\eta}\right)^2 + \frac{k_4}{c_{44}^s} \lambda^2 - \frac{\rho}{\rho^s} \Omega^2 & -\lambda \frac{k_2 + c_{66}}{c_{44}^s} \frac{n}{\eta} & -\beta_2 \lambda & -\gamma_2 \lambda \sqrt{\frac{\chi_{33}^s}{c_{44}^s}} \\ -\lambda \frac{k_3 + c_{66}}{c_{44}^s} \frac{n}{\eta} & \frac{k_1}{c_{44}^s} \frac{n^2}{\eta^2} + \frac{c_{66}}{c_{44}^s} \lambda^2 - \frac{\rho}{\rho^s} \Omega^2 & \beta_1 \frac{n}{\eta} & \gamma_1 \sqrt{\frac{\chi_{33}^s}{c_{44}^s}} \frac{n}{\eta} \\ \beta_2 \lambda & -\beta_1 \frac{n}{\eta} & \frac{\chi_{33}}{\alpha} c_{44}^s & \frac{e_{33}}{\alpha} \sqrt{c_{44}^s \chi_{33}^s} \\ \gamma_2 \lambda \sqrt{\frac{\chi_{33}^s}{c_{44}^s}} & -\gamma_1 \sqrt{\frac{\chi_{33}^s}{c_{44}^s}} \frac{n}{\eta} & \frac{e_{33}}{\alpha} \sqrt{c_{44}^s \chi_{33}^s} & \frac{c_{33} \chi_{33}^s}{\alpha} \end{bmatrix}$$

$$\mathbf{D}_{22} = \begin{bmatrix} -\frac{1}{\eta} & 0 & -\frac{k_2}{c_{44}^s} \frac{\lambda}{\eta} & 0 \\ 0 & -\frac{2}{\eta} & \frac{k_1}{c_{44}^s} \frac{n}{\eta^2} & 0 \\ 0 & 0 & -\beta_1 \frac{1}{\eta} & 0 \\ 0 & 0 & -\gamma_1 \sqrt{\frac{\chi_{33}^s}{c_{44}^s}} \frac{1}{\eta} & 0 \end{bmatrix}$$

where

$$\begin{aligned} \alpha &= c_{33} \chi_{33} + e_{33}^2, \quad \beta_1 = (c_{13} \chi_{33} + e_{31} e_{33}) / \alpha, \quad \beta_2 = (c_{23} \chi_{33} + e_{32} e_{33}) / \alpha \\ \gamma_1 &= (c_{13} e_{33} - c_{33} e_{31}) / \alpha, \quad \gamma_2 = (c_{23} e_{33} - c_{33} e_{32}) / \alpha, \quad k_1 = c_{11} - c_{13} \beta_1 - e_{31} \gamma_1 \\ k_2 &= c_{12} - c_{23} \beta_1 - e_{32} \gamma_1, \quad k_3 = c_{12} - c_{13} \beta_2 - e_{31} \gamma_2, \quad k_4 = c_{22} - c_{23} \beta_2 - e_{32} \gamma_2 \\ k_5 &= \chi_{11} + e_{15}^2 / c_{55}, \quad k_6 = \chi_{22} + e_{24}^2 / c_{44}, \quad \lambda = m \pi R / L, \quad \Omega = \omega R \sqrt{\rho^s / c_{44}^s} \end{aligned} \tag{A2-4}$$